JOURNAL OF GEOPHYSICAL RESEARCH, VOL. 117, A07312, doi:10.1029/2011JA017454, 2012

Longitudinal differences of ionospheric vertical density distribution and equatorial electrodynamics

E. Yizengaw,[1] E. Zesta,[2] M. B. Moldwin,[3] B. Damtie,[4] A. Mebrahtu,[5] C. E. Valladares,[1] and R. F. Pfaff[6]

Received 14 December 2011; revised 17 May 2012; accepted 30 May 2012; published 19 July 2012.

[1] Accurate estimation of global vertical distribution of ionospheric and plasmaspheric density as a function of local time, season, and magnetic activity is required to improve the operation of space-based navigation and communication systems. The vertical density distribution, especially at low and equatorial latitudes, is governed by the equatorial electrodynamics that produces a vertical driving force. The vertical structure of the equatorial density distribution can be observed by using tomographic reconstruction techniques on ground-based global positioning system (GPS) total electron content (TEC). Similarly, the vertical drift, which is one of the driving mechanisms that govern equatorial electrodynamics and strongly affect the structure and dynamics of the ionosphere in the low/midlatitude region, can be estimated using ground magnetometer observations. We present tomographically reconstructed density distribution and the corresponding vertical drifts at two different longitudes: the East African and west South American sectors. Chains of GPS stations in the east African and west South American longitudinal sectors, covering the equatorial anomaly region of meridian ~37°E and 290°E, respectively, are used to reconstruct the vertical density distribution. Similarly, magnetometer sites of African Meridian B-field Education and Research (AMBER) and INTERMAGNET for the east African sector and South American Meridional B-field Array (SAMBA) and Low Latitude Ionospheric Sensor Network (LISN) are used to estimate the vertical drift velocity at two distinct longitudes. The comparison between the reconstructed and Jicamarca Incoherent Scatter Radar (ISR) measured density profiles shows excellent agreement, demonstrating the usefulness of tomographic reconstruction technique in providing the vertical density distribution at different longitudes. Similarly, the comparison between magnetometer estimated vertical drift and other independent drift observation, such as from VEFI onboard Communication/Navigation Outage Forecasting System (C/NOFS) satellite and JULIA radar, is equally promising. The observations at different longitudes suggest that the vertical drift velocities and the vertical density distribution have significant longitudinal differences; especially the equatorial anomaly peaks expand to higher latitudes more in American sector than the African sector, indicating that the vertical drift in the American sector is stronger than the African sector.

Citation: Yizengaw, E., E. Zesta, M. B. Moldwin, B. Damtie, A. Mebrahtu, C. E. Valladares, and R. F. Pfaff (2012), Longitudinal differences of ionospheric vertical density distribution and equatorial electrodynamics, *J. Geophys. Res.*, *117*, A07312, doi:10.1029/2011JA017454.

[1]Institute for Scientific Research, Boston College, Chestnut Hill, Massachusetts, USA.
[2]Air Force Research Laboratory, AFRL/VSBXP, Hanscom AFB, Bedford, Massachusetts, USA.
[3]Department of Atmospheric, Oceanic and Space Sciences, University of Michigan, Ann Arbor, Michigan, USA.
[4]Washera Geospace and Radar Science Laboratory, Bahir Dar University, Bahir Dar, Ethiopia.
[5]Department of Physics, Mekelle University, Mekelle, Ethiopia.
[6]NASA Goddard Space Flight Center, Greenbelt, Maryland, USA.

Corresponding author: E. Yizengaw, Institute for Scientific Research, Boston College, 140 Commonwealth Ave., Chestnut Hill, MA 02467, USA. (endawoke.kassie@bc.edu)

0148-0227/12/2011JA017454

1. Introduction

[2] The uneven distribution of ground-based instruments due to oceans hinders our ability to obtain a global understanding of the dynamics and structure of the equatorial ionosphere. Over oceans and under-instrumented regions, like Africa, the ionospheric density structure has been traditionally estimated by model interpolation over vast geographic areas, and that make difficult for the communication and navigation systems operating in the region. Knowledge of the ionospheric electron density distribution is very important for many technologies, such as estimation and correction of propagation delays in global positioning systems (GPS) navigation system [e.g., *Kintner et al.*, 2009],

ionospheric storm studies [e.g., *Yizengaw et al.*, 2005; *Basu et al.*, 2009], ion composition studies [e.g., *Immel et al.*, 2006], space-weather effects on telecommunications [e.g., *Doherty et al.*, 2004] and many more. However, the distribution of electron density throughout the ionosphere shows complicated structure, exhibiting different types of structures and gradients at different longitudinal sectors [e.g., *Immel et al.*, 2006]. Such complicated density structures at different longitudes makes modeling a challenging task. For many years a variety of techniques and systems have been developed and used to study the density distribution in the ionosphere. Radio wave transmission and reception at fixed locations on the ground, such as pulsed HF ionosonde and incoherent scatter radar (ISR) [e.g., *Foster*, 1993], topside sounder onboard satellite [e.g., *Reinisch et al.*, 2001], and in situ rocket and satellite observations [e.g., *Stankov et al.*, 2003] are among those different techniques that have been used to study the vertical electron density of the ionosphere. However, these instruments are sparsely located and it is impossible to image the global density structures using these instruments for two main reasons: (1) they are too expensive to place at different longitudinal sector, and (2) they only provide density profiles up to a certain altitude. In order to image the structure and dynamics of ionospheric density continuously, the tomographic inversion method (based on a linear mathematical inversion) can be applied to GPS total electron content (TEC) measurement whereby a number of existing transmitters on the ground and on board Low-Earth-Orbiting (LEO) satellites are used to provide TEC values. A full description of the TEC extraction methods can be found in [e.g., *Mannucci et al.*, 1998; *Yizengaw et al.*, 2004].

[3] At mid- and low-latitudes the effects of vertical $\mathbf{E} \times \mathbf{B}$ drifts begin to strongly influence ionospheric structure [e.g., *Anderson et al.*, 2004]. The strong drift lifts the plasma at the equator and then moves it down along the magnetic field lines to higher latitudes by the pressure gradient and gravity forces, forming a clear equatorial anomaly. A variable vertical drift velocity may cause different density distributions at different longitudes. *Anderson and Araujo-Pradere* [2010], using magnetometer data clearly demonstrated that the vertical drift has a significant magnitude difference at different longitudes. Using in situ density observation at a fixed altitude or ground-based integrated density observations different groups reported the longitudinal density distribution differences, which are mainly focused not on the EIA structure longitudinal difference but on the formation of wave number four structures [*England et al.*, 2010, and references therein]. Similarly, *Lin et al.* [2007], using two months (July and August 2006) average COSMIC occultation profiles, reported longitudinal dependence of the vertical density profiles of the ionosphere. However, the day-to-day vertical density distribution difference at different longitudes, primarily at low and equatorial latitudes, has not been investigated, despite some ground-based instruments that are sparsely located around the world. Thus, for the first time, we present the day-to-day variability of the density distribution difference between African and American sectors using data from the recently deployed instruments.

[4] This paper presents, for the first time, simultaneous observations of both the vertical density distribution at low and equatorial latitudes and the corresponding driving vertical drift at two longitudinal sectors. The vertical density structures are obtained by applying a tomographic inversion technique to the collection of GPS slant TEC recorded by a chain of GPS receivers. At the same time, the magnitude and direction of the vertical drift ($\mathbf{E} \times \mathbf{B}$ drift) velocities can be estimated using ground-based magnetometer arrays [*Anderson et al.*, 2004; *Yizengaw et al.*, 2011]. This is possible since the difference between the horizontal component magnetic field (H) at the equator and at a non-equatorial location is a good indicator of the equatorial electrojet [*Anderson et al.*, 2004] and thus the vertical $\mathbf{E} \times \mathbf{B}$ drift [*Anderson et al.*, 2004; *Yizengaw et al.*, 2011]. The combination of global density distribution and global vertical drifts can lead to the global monitoring of equatorial electrodynamics with an advantageous spatial scale.

2. Tomography

[5] The GPS constellation currently consists of 29 satellites orbiting at ~55° inclination in six distinct orbital planes and at ~20,200 km altitude (~4.2 L). Each satellite broadcasts two L-band signals at frequencies $f_1 = 1.57542$ *GHz* and $f_2 = 1.2276$ *GHz.* Owing to the dispersive nature of the ionosphere, dual frequency GPS measurements can provide integral information about the ionosphere and plasmasphere by computing the differential phases of the code and carrier phase measurements recorded at the ground-based GPS receivers [*Klobuchar*, 1996]. Details of TEC calculation from GPS observations are described in several papers [e.g., *Yizengaw et al.*, 2004; and references therein]. TEC measurements provide only the line integral of the free electron density along individual lines of sight, but offer no information on the vertical profile of the density structures. However, the fact that multiple TEC lines of sight are available at any instant at a single Earth location allows the determination of the full vertical density profile by a tomographic inversion method (based on a linear mathematical inversion) [*Heise et al.*, 2002; *Yizengaw et al.*, 2007 and the reference therein]. The tomographic inversion essentially obtains maps of the altitude distribution of electron density from the collection of GPS slant TEC observations obtained across a region. The reconstruction plane is discretized into two-dimensional pixels [*Heise et al.*, 2002; *Yizengaw and Moldwin*, 2005]. Usually, but not necessarily, the grid of these two-dimensional boxes is subdivided equidistantly with height and angular spacing [e.g., *Yizengaw et al.*, 2007]. By representing as a finite sum of shorter integrals along segments of the raypath length in each pixel, and assuming that the electron density is constant in each pixel [*Tsai et al.*, 2002] the integrated GPS TEC can be inverted into vertical density distribution. Figure 1 shows the location of the GPS receivers (sold red circles) in the east African and west South American sectors used for this study. The vertical dashed lines along each set of stations denote the location of the tomography reconstruction vertical plane of each meridian of interest.

[6] We use the algebraic reconstruction technique (ART) to invert the GPS slant TEC (STEC) into vertical density profiles. Detailed description of the ART algorithm and discussion about the potential and limitations of the technique, can be found [e.g., *Na et al.*, 1995; *Pryse et al.*, 1995; *Raymund*, 1995]. The ART algorithm is an iterative algorithm that uses the row projection technique, and requires an

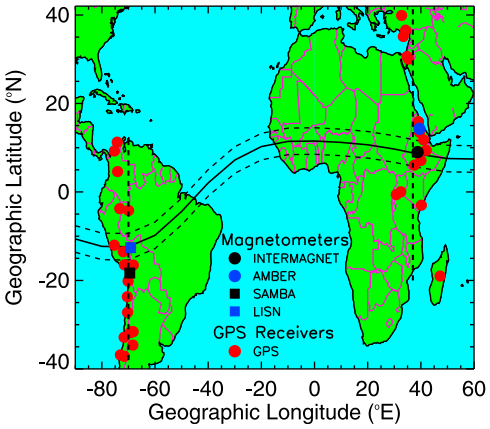

Figure 1. Geographic location of the ground-based magnetometers and GPS receivers used for this study. The solid horizontal line depicts the geomagnetic equator, and the two dashed lines indicate the EEJ region.

initial density profile guess as input. We use a combination of the Chapman profile (for top side ionosphere) and the IRI model (for bottomside ionosphere) as our initial profile. The ART algorithm is the most widely used algorithm [e.g., *Mitchell et al.*, 1997; *Pokhotelov et al.*, 2008; *Bust and Mitchell*, 2008 and there reference therein], and it converges quickly compared to other reconstruction algorithms. This makes it the most preferable algorithm to use in regions with limited number of widely spaced receivers, like the GPS receiver network in the African sector.

[7] In addition to the already known factors that limits ionospheric tomographic reconstruction, such as, the number of raypaths between the transmitters and receivers, the way the region of interest is intersected by the rays (i.e., whether the available raypaths are distributed across the region of interest uniformly or not), the time required to complete the data sampling and GPS satellite geometry are also other factors for ionospheric tomography. Typically, tomographic algorithms assume that the data measurement paths and the region of interest are coplanar. In the case of GPS ionospheric tomography, however, the chain of receivers, the ionospheric region of interest, and the spacecraft orbit are not necessarily entirely coplanar. Thus the TEC raypaths may have passed through the regions of ionosphere far different from the desired imaging plane. If the set of TEC data does not accurately reflect the ionosphere in the plane of interest, reconstructions obtained from the data should be expected to differ in some way from other independent measurements, such as ionosonde and Incoherent Scattering Radar (ISR) density profiles. Therefore, in order to address such geometry problems, all GPS raypaths from all satellites that were in view to the chain of receivers in the region of interest are not entirely used for the inversion process. Instead, data obtained only from a number of suitable satellite passes viewed by the available receivers near the plane of interest are used. In this particular study for our ground-based tomography we include data only from those GPS satellites that are within $\pm 30^\circ$ longitude from the meridian of the chain of receivers. For the relatively short sampling period of 25–30 min, longitudinal density differences in between $\pm 30^\circ$, from the satellite altitude, is assumed insignificant and can be ignored. Thus, the raypath from the satellite at 30 degree away has a horizontal distance of about 230 km between its projection from the median density peak height ($\sim$400 km) and the meridian longitudes, indicating the local time gap encompassed by the tomography gets shorter at the ionospheric density peak altitude. This strengthens the validity of the $\pm 30^\circ$ cut off longitude criteria, because the density above about 1200 km is insignificant for ionospheric tomographic reconstruction. Moreover, the ionosphere generally varies much more rapidly with latitude than longitude. With this assumption we then merge the raypaths combined from those suitable satellites, based on the restriction mentioned above, into two-dimensions along the meridian of the chain of receivers. For example, if the meridian of chain of receivers is 37°E and a GPS satellite that provides data for the reconstruction process is located at (−25°N, 54°E, 20200 km), then in order to make the data measurement paths and the region of interest in the same plane, the new satellite position will be shifted to (−25°N, 37°E, 20200 km). Simply, the longitudes of the satellites are shifted to the meridian of the receivers by keeping their latitudes, altitudes, and slant TEC values unchanged.

3. Vertical Drift

[8] The magnitude and direction of the dayside vertical velocity ($\mathbf{E} \times \mathbf{B}$ drift) can be easily estimated using pairs of ground magnetometers around the dip equator [*Anderson et al.*, 2004, 2006; *Yizengaw et al.*, 2011]. The equatorial electrojet current (EEJ) produces a strong enhancement in the *H*-component magnetic field measured by magnetometers located within $\pm 5^\circ$ of the magnetic equator. In principle, measuring this perturbation in equatorial magnetometers could provide a direct measure of the EEJ. However, ground magnetometers respond to all currents within their field of view. Equatorial stations respond primarily to the EEJ, which is directly overhead, but also to the ring current and the global quiet time Sq current system. The typical extent of the EEJ is to within $\pm 5^\circ$ of the dip equator. Ground magnetometers just outside the extent of the EEJ, 6°–9° off the dip equator, would exhibit near-zero response to the EEJ, but have the exact response to the ring and Sq currents as an equatorial station, because those currents are much further away from both stations. The ring current and global Sq dynamo contribution to the *H*-component can then be removed from the *H*-component field by subtracting the *H*-component recorded at the off the equator ($\sim$6–9° geomagnetic) magnetometer ($\Delta H_{non-equ}$) from the *H*-component value measured at the magnetic equator (ΔH_{equ}). The difference is the only part of the *H*-component field that is related to the EEJ current contribution which, in turn, is directly related to the east–west electric field that triggered the system to create the electrojet current. Therefore, the $\mathbf{E} \times \mathbf{B}$ drift can be estimated using the resulting ΔH ($\Delta H = \Delta H_{equ} - \Delta H_{non-equ}$) value of the *H*-component field [see *Anderson et al.*, 2004]. To avoid different offset values of different magnetometers, the nighttime baseline values in the H component are first obtained for each day and subtracted from the corresponding magnetometer data sets. This provides the variation of daytime H-component values (ΔH) of each magnetometer.

[9] For the estimation of drifts in this study, the African sector, ($\sim$37°E longitude) pair of magnetometers consists of

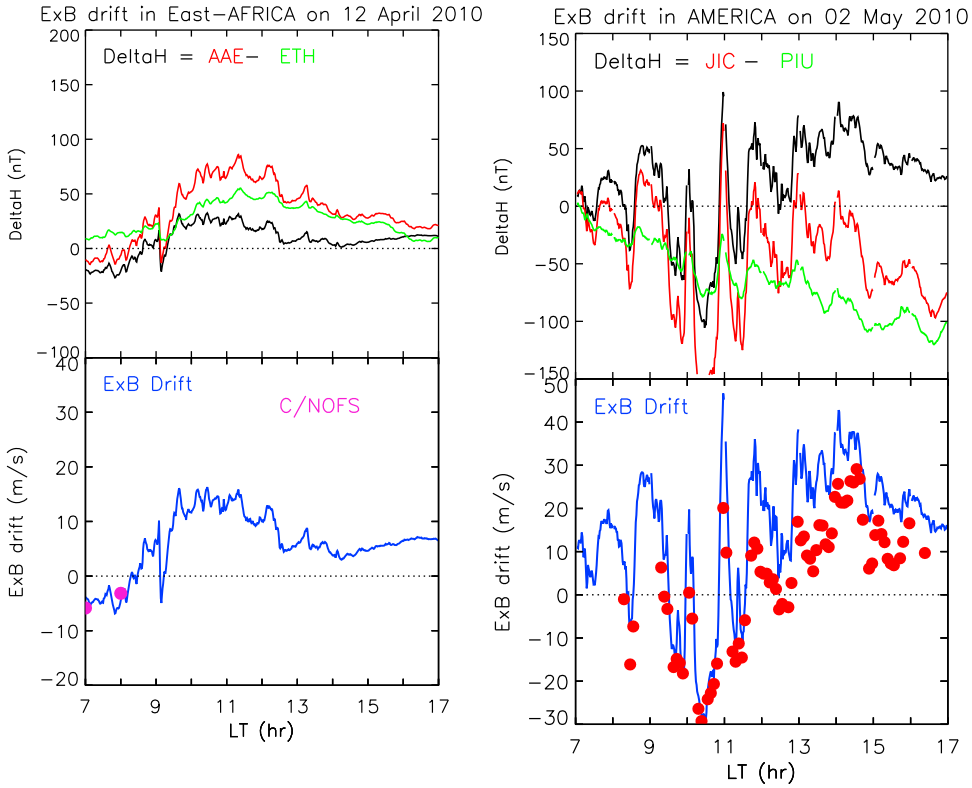

Figure 2. The top plots show the magnetic fluctuation recorded at the geomagnetic equator (red curves) and off the magnetic equator (green curves) and the difference between red and green curve, ΔH (black curve). The bottom plots show an estimated $\mathbf{E} \times \mathbf{B}$ drift (blue curve), and pink and red dots represent vertical drift velocity observed by VEFI instrument onboard C/NOFS satellite and JULIA 150 km radar, respectively. Observations performed in the (left) African and (right) American sectors.

the Adigrat station (14.28°N, 39.46°E geographic, 6.0°N, 111.06°E geomagnetic) of the AMBER chain and the Addis Ababa station (9.04°N, 38.77°E geographic, 0.17°N, 110.47°E geomagnetic) of the INTERMAGNET network. The South American sector pair consists of the Putre station (−18.33°N, −69.50°E geographic, −5.50°N, 1.44°E geomagnetic) of the SAMBA chain and the Puerto Maldonado station (−12.59°N, −69.19°E geographic, 0.02°N, 2.03°E geomagnetic) of the LISN chain. Figure 1 shows, as black and blue squares and circles, the geographic location of the ground-based instruments used for this study. We also used the Jicamarca (−11.95°N, −76.87°E geographic, 0.61°N, −5.4°E geomagnetic) and Piura (−5.17°N, −80.64°E geographic, 6.8°N, −9.4°E geomagnetic) magnetometer pair to estimate the dayside vertical drift velocity.

4. Results and Discussion

[10] Figure 2 shows a typical example of equatorial drifts estimated from magnetometer pairs in the African sector (Figure 2, left) and American sector (Figure 2, right) for a geomagnetically active days on 12 April, 2010 and on 2 May, 2010, respectively. The top plots show the magnetic field variation recorded by the magnetometers located at the geomagnetic equator (red curve) and off the equator (green curve). The black curve is the difference between the red and green curves (ΔH), representing the isolated effect of the equatorial electrojet current. The blue curve in the bottom plot is the $\mathbf{E} \times \mathbf{B}$ drift estimated from the corresponding ΔH values (black curve in the top plot), using the technique described in *Anderson et al.* [2004]. In order to reaffirm the validity of the magnetometer drift estimation technique, we compared the magnetometer estimated $\mathbf{E} \times \mathbf{B}$ drift with other independently measured drift velocities, specifically with C/NOFS observations over the African sector and with the Jicamarca's JULIA radar over the South American sector. Although there are only two data points only in the morning side, the comparisons with the C/NOFS observations in the African sector (Figure 2, bottom left) are very good. In the comparison with the 150 km echoes of the JULIA radar (red dots in Figure 2, bottom right) the magnetometer estimated drifts have an excellent agreement with the radar drifts in the morning hours but seem to overestimate the magnitude of the drifts in the afternoon hours. Nevertheless, the magnetometer estimated drifts reproduce all the fluctuations observed by the radar at all local times confirming that the magnetometer technique works well even for small scale drift fluctuations. The 40–60 min periodic fluctuations shown on both magnetometer estimated and radar measurements could be due to a periodic wave that penetrates from the magnetosphere and modulates the equatorial *E* region electrodynamics. Detailed information about such type of drift fluctuations can be found in [*Yizengaw et al.*, 2011], and thus we will not discuss this topic further in this paper.

[11] In order to obtain the vertical density distribution, we applied the tomographic inversion technique to the slant TEC

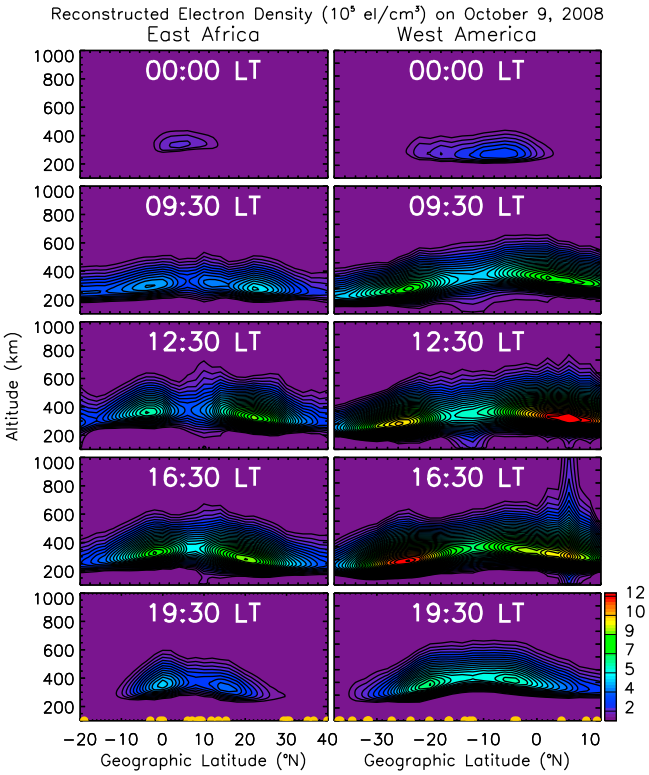

Figure 3. Tomographically reconstructed ionospheric electron density profiles in altitude versus geographic latitude for 9 October 2008. Shown are density profiles in the (left) African and (right) American sectors. Each plot from top to bottom depicts density profiles at different local times.

measured by the chain of stations lined up at the meridian of ~37°E (east African sector) and 290°E (west South American sector). These meridian sectors are identified at the median longitudes of all the stations of each longitudinal sector. Figure 3 shows the vertical density distribution of the ionosphere at the two different longitudinal sectors produced by tomographic reconstruction technique, based on the criteria mentioned above, for 9 October 2008. Figure 3 shows the density distribution in the east African and west South American sectors and for different local times. The altitude versus geographic latitude density distribution shows clear large-scale structures, such as the evolution of equatorial ionospheric anomaly (EIA) formation. There is no EIA during local midnight, it is weaker in the morning and stronger around noon and afternoon. The yellow dots at the bottom panel indicate the latitudinal distribution of the chain of GPS stations used to produce the density distribution shown in each panel. Differences between the two longitudes are also evident, with significantly higher density in the American sector than in the African sector. We have generated a number of similar images of density distribution during different magnetic activity periods and found similar density distribution differences between these two longitudinal sectors. Obviously, the two longitudinal sectors have different geographic and geomagnetic equator alignments. While the American sector has fairly large excursions between the geomagnetic and geographic equator, the African sector has only a very small excursion between the geomagnetic and geographic equators. Such different excursion could be responsible [*Kintner et al.*, 2009] for different equatorial electrodynamics and thus density distribution often observed between the African and American sectors.

[12] Another point of interest in Figure 3 is the F2-peak density altitude difference between southern and northern EIA crest, which is clearly visible on the dayside, primarily around noon and in the afternoon sector. In the African sector the EIA peak in the southern hemisphere appears to be at higher altitude (at ~350 km) than that in the northern hemisphere (at ~310 km). On the other hand, in the American sector trans-equatorial meridional the EIA peak in the northern hemisphere occurs at a higher altitude (at ~315 km) compared to the EIA peak in the southern hemisphere, which is at ~275 km. This could be due to the difference in the trans-equatorial meridional wind orientation at the different regions. In the African sector the trans-equatorial meridional wind looks from southern to northern hemisphere, raising the plasma along the magnetic field in the southern hemisphere and driving it down in the northern hemisphere in the African sector. On the other hand, trans-equatorial meridional wind orients from northern to southern hemisphere, causing the northern and southern hemisphere peaks to be at higher and lower altitudes, respectively. Similar different meridional wind orientation that leads to the anomaly peak difference between East and Westside of South American has been often observed [*Valladares and Chau*, 2012]. Equatorward winds lift plasma to higher altitudes whereas poleward winds drive plasma to lower altitudes along the magnetic field line [e.g., *Jakowski et al.*, 1999]. Figure 3 demonstrates the strength of our analysis that can enable us to investigate these types of local dynamics.

[13] Next, we validate our technique by comparing tomographically obtained ionospheric density profiles with Jicamarca ISR density profiles. First we produce a series of altitude versus latitude density profiles, shown in Figure 3, for the entire day at 30 min intervals, and then extract the density profiles at a fixed latitude as a function of time so that we can have the diurnal vertical density distribution of the ionosphere at a fixed latitude, which enables the direct comparison with the Jicamarca ISR, located at ~290°E longitude and ~−12.0°N latitude. Figure 4 shows the comparison between tomographically reconstructed (Figure 4, top) and available ISR (Figure 4, bottom) density profiles at the 290°E meridian during 29 October, 2008, which is one of the two days where Jicamarca radar was running in oblique mode in the entire October 2008. The white curve over plotted on both panels represents the vertical drift velocity estimated from the Jicamarca – Piura pair of magnetometers. The white horizontal dashed curves show the zero level of the vertical drift velocity of its scale shown on the right side of Figure 4. The 00 MLT is also marked with a vertical white line in Figure 4 (top). The two independent measurements show excellent agreement both in density magnitude, structure, and peak altitudes, demonstrating the power of the tomographic reconstruction technique that can satisfactorily image the vertical density distribution in a cost effective way. We have performed several days of comparison during different season but due to limited space we only present one example to demonstrate the tomographic reconstruction techniques can provide reasonable samples of the ionospheric density structure.

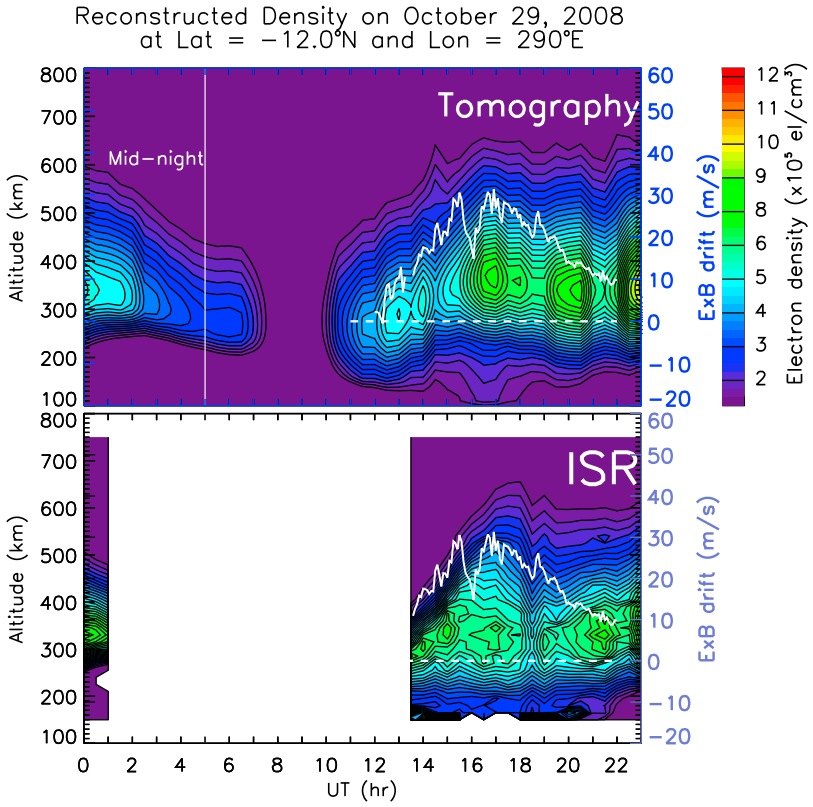

Figure 4. The vertical electron density distribution at 290°E longitude and −12°N latitude location, obtained (top) by tomographic reconstruction technique and (bottom) by Jicamarca ISR. The over plotted white curves (scale shown at the right) depict the vertical **E** × **B** drift estimated using magnetometer data. Data were not available during the time gap shown by the white area in Figure 4 (bottom).

[14] Monitoring the vertical density profile simultaneously with the plasma drifts can be a powerful and comprehensive tool in understanding the equatorial electrodynamics. Transport is one of the mechanisms that can cause plasma redistribution. The equatorial vertical drift is one of the most important driving mechanisms for ionospheric density redistribution. Figure 5 shows simultaneous observations of the time development of tomographically inverted vertical density profiles and magnetometer estimated vertical drifts on 19 October, 2008 (similar format to Figure 4). October 19 is chosen just because we had drift observations on both longitudes. The top row shows the density distribution at the southern EIA peak, geomagnetic equator, and northern EIA peak regions observed in the American sector. Figure 5 (bottom) is the same as Figure 5 (top) but for the African sector. The magnetometer-estimated vertical drift is from the equatorial pair of magnetometers but is overplotted at all latitude panels for the appropriate longitude sector. The density gets low at the geomagnetic equator and enhanced at the EIA peaks at both longitude sectors, which is consistent with the fountain effect principles. The vertical drift lifts the plasma to higher altitudes, where it can survive a long time due to reduced recombination, and then drifts down to higher latitudes along the geomagnetic field. In the South American sector (Figure 5, top) the density depletion at the equator responds quickly to the vertical drift velocity compared to the density enhancement at the EIA peaks. The onset of the density enhancement at the peaks occurs approximately 1 h after the maximum density depletion (centered at about 16:00 UT in the top middle panel) is observed at the equator, which is likely due to the time required for lift and meridional transport. In the African sector (bottom panels), however, the vertical drift velocity exhibited a counter electrojet (downward drift) for an extended period of the dayside (8:00–14:00 UT or 11:00–17:00 LT). At the same time the density distribution at the geomagnetic equator is severely depleted. We believe that this is due to the downward drift velocity that pushed the plasma to lower altitudes where the recombination rate is high [e.g., *Yizengaw et al.*, 2011]. Similarly, there was no significant density enhancement observed at the anomaly peak region during the dayside counter electrojet event, even the noon local time density at the southern EIA peak region goes down to early morning density levels often observed during normal and geomagnetically quiet days. Generally, for the simultaneous observation of density distributions and vertical drift velocities at two distinct longitudes, the stronger the drift velocity, the stronger the density transport and formation of significant density depletion and enhancement at the geomagnetic equator and EIA peak regions, respectively. Thus, the density enhancements at the EIA crest region was more pronounced in the American sector where we observed the strongest **E** × **B** drifts, compared to the African sector where we observed downward **E** × **B** drifts. This clearly demonstrates that the equatorial vertical drift is indeed governing

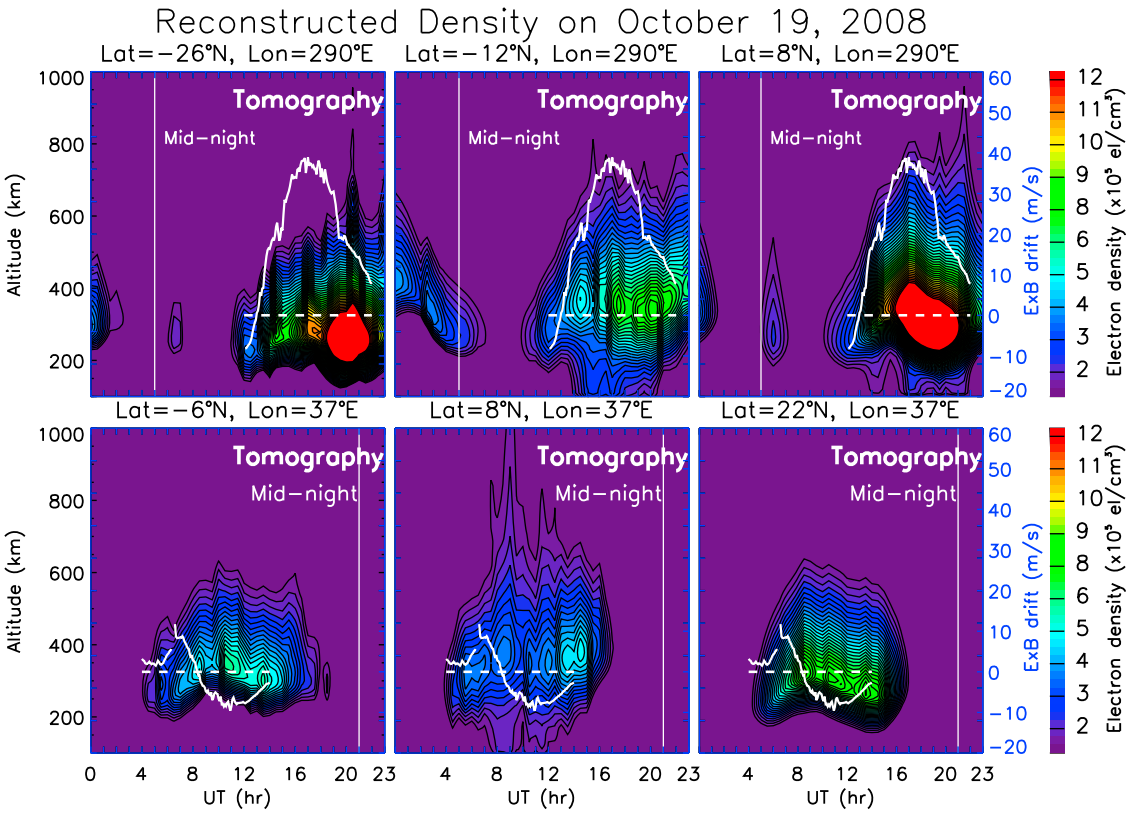

Figure 5. As for Figure 4 but for reconstruction performed (top) at 290°E and (bottom) at 37°E meridian sectors. The plots in the first row represent density profiles at different latitudes: −26°N (southern side equatorial anomaly peak region), −12°N (geomagnetic equator), and 8°N (northern side equatorial anomaly peak region) latitudes at 290°E meridian. Similarly, the plots in the second row represent the density profiles at −6°N (southern side equatorial anomaly peak region), 8°N (geomagnetic equator), and 22°N (northern side equatorial anomaly peak region) latitudes at 37°E meridian. The white curves indicate the vertical **E** × **B** drift velocity of scale shown at the right.

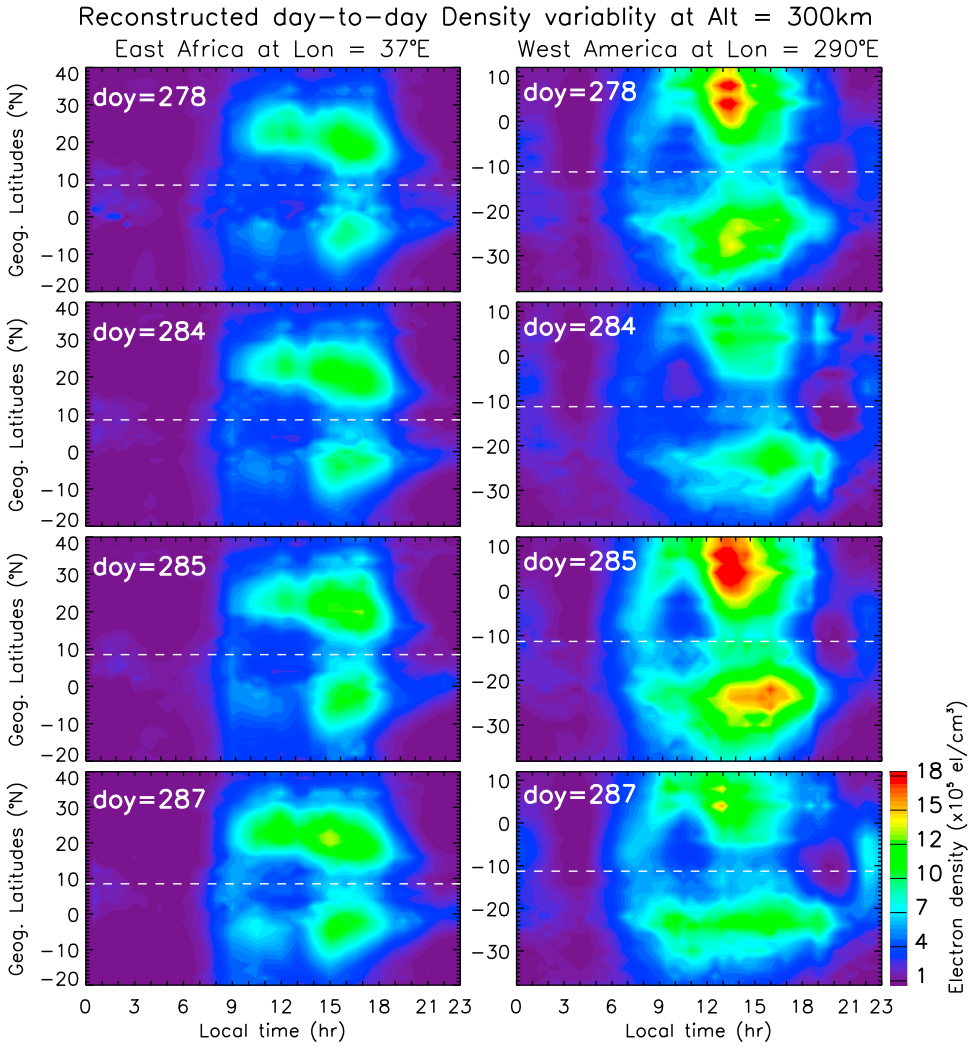

Figure 6. The latitude versus local time cut of the density that shows day-to-day variability of the ionosphere at an altitude of 300 km. Shown are the density variabilities on different days in the (left) African and (right) American sectors.

electrodynamics of the equatorial ionosphere as a function of latitude (or *L-shell*), local time, longitude, and magnetic activity.

[15] Tomographic reconstruction allows us to track the dynamics of the vertical density profile at a particular longitude and latitude as was done in Figures 4 and 5, but can also track the density dynamic evolution with respect to latitude at a fixed altitude, which can help us understand the latitudinal transport of equatorial plasma. Figure 6 shows density as function of latitude and time at 300 km altitude obtained from the tomographically imaged vertical density distributions for different days in October 2008. Figure 6 (left) represents the density over Africa and Figure 6 (right) shows the density in the American sector. A dramatic density difference is seen between the American and African longitudes, with density significantly larger in the American than African sectors. Moreover, the clearly visible day-to-day variability of the density structure shown in Figure 6 could be attributed to the different level of ionization for each day due to different solar forcing because of different geomagnetic activities. For example, the daily *Kp* sums for day 278, 284, 285, and 287 are 17, 5, 30, and 15, respectively. This clearly shows the higher the daily *Kp* indicates higher photoionization (due to the flares that precede the *Kp* index enhancement) and the associated transport that could produce density enhancement in the ionosphere which is consistent with the day-to-day density distributions shown in Figure 6. Nevertheless, in both longitudes the southern EIA peak is weaker than the northern peak. The advantage of this type of visualization of tomographic densities is its convenience in comparing and validating in situ densities observed by LEO satellites. We do exactly that in Figure 7, where we compare in situ densities measured by the Planar Lagmuir Probe (PLP) onboard the C/NOFS satellite with those determined by tomographic inversion at the location of the satellite. Figure 7 (top) shows the PLP's in situ density, observed when C/NOFS was below 450 km altitude, over Africa and South America for limited passes. The local time distribution of these passes is shown in middle panel and its traces onto the latitude versus local time cut of the tomographically reconstructed density at 420 km altitude is shown in the third panel from the top. The bottom panel shows the line plot comparison between in situ (red

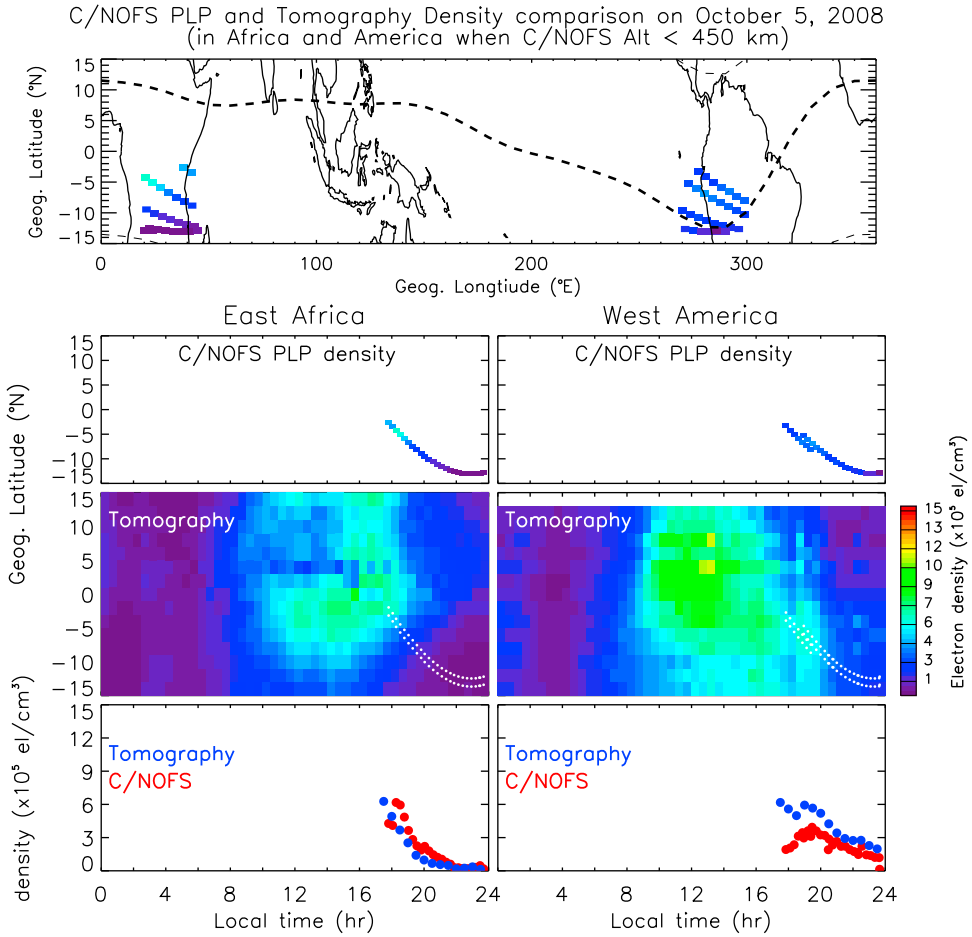

Figure 7. The first row shows the C/NOFS PLP in situ density over Africa and south America for limited passes and when the satellite was below 450 km altitude, the second row shows the local time distribution of the satellite passes shown in the first row, and the third row shows the latitude versus local time cut of the tomographically reconstructed density at 420 km altitude. The white dots in the third row indicate the traces of C/NOFS PLP density local time distribution shown in the second row, and the fourth row shows a line plot comparison between in situ (red dots) density and the tomography profile (blue dots) extracted along the white trace shown in the third row.

dots) density and the tomographically imaged density profiles (blue dots) extracted along the white trace shown in the third panel. In general, the comparison between C/NOFS and tomographically reconstructed densities show excellent agreement, especially in the African sector. However, in the American sector there is significant difference between the two at earlier time (1700–1930 UT), and C/NOFS's density lower than the tomography.

5. Conclusion

[16] In conclusion, the GPS tomographic inversion technique is an effective means of producing vertical ionospheric density distributions over a very wide area of coverage and in a cost-effective way. It is a potential means to probe the ionosphere on a number of spatial and temporal scales to examine the different aspects of the structure and variability of ionospheric density at different longitudinal sectors. The comparison between tomographically imaged and ISR measured density distributions clearly demonstrate the capability of the tomographic reconstruction technique. It reveals the clear and significant density differences between east African and west South American sectors. From our several months of observation, the ionospheric density in the east African sector always appears to be significantly weaker in magnitude compared to that of the American sector. However, further analysis, such as seasonal variability, is required to clearly understand the physics behind for such longitudinal density distribution. Similarly, the vertical drift velocity, which was simultaneously estimated using magnetometer observations, also show weak vertical drift velocity in the African sector compared to the American sector. The equatorial anomaly peaks also expand to higher latitudes more in American sector than the African sector (see Figures 3 and 6), indicating that the vertical drift in the American sector is stronger than the African sector. Simultaneous investigation of such longitudinal density distribution as well as drift velocities for the first time could contribute significantly to the efforts of space weather dependent global ionospheric density modeling, and thus improve our communication and navigation systems.

[17] **Acknowledgments.** This work was supported by NASA IHY (NNX07AM22G), LWS (NNX11AP02G and NNX10AQ53G) and Geospace Science programs (NNX09AR84G) and AFOSR YIP grant (FA9550-10-1-0096). The authors are indebted to the IGS and UNAVCO GPS, Jicamarca radar, and INTERMAGNET magnetometer teams for the data resources they made available to the public.

[18] Robert Lysak thanks the reviewers for their assistance in evaluating this paper.

References

Anderson, D., and E. A. Araujo-Pradere (2010), Sudden stratospheric warming event signatures in daytime **E** × **B** drift velocities in the Peruvian and Philippine longitude sectors for January 2003 and 2004, *J. Geophys. Res.*, *115*, A00G05, doi:10.1029/2010JA015337.

Anderson, D., A. Anghel, J. Chau, and O. Veliz (2004), Daytime vertical **E** × **B** drift velocities inferred from ground-based magnetometer observations at low latitudes, *Space Weather*, *2*, S11001, doi:10.1029/2004SW000095.

Anderson, D., A. Anghel, J. L. Chau, and K. Yumoto (2006), Global, low-latitude, vertical **E** × **B** drift velocities inferred from daytime magnetometer observations, *Space Weather*, *4*, S08003, doi:10.1029/2005SW000193.

Basu, Su., S. Basu, J. Huba, J. Krall, S. E. McDonald, J. J. Makela, E. S. Miller, S. Ray, and K. Groves (2009), Day-to-day variability of the equatorial ionization anomaly and scintillations at dusk observed by GUVI and modeling by SAMI3, *J. Geophys. Res.*, *114*, A04302, doi:10.1029/2008JA013899.

Bust, G. S., and C. N. Mitchell (2008), History, current state, and future directions of ionospheric imaging, *Rev. Geophys.*, *46*, RG1003, doi:10.1029/2006RG000212.

Doherty, P., A. J. Coster, and W. Murtagh (2004), Space weather effects of October–November 2003, *GPS Solutions*, *8*(4), 267–271, doi:10.1007/s10291-004-0109-3.

England, S. L., T. J. Immel, J. D. Huba, M. E. Hagan, A. Maute, and R. DeMajistre (2010), Modeling of multiple effects of atmospheric tides on the ionosphere: An examination of possible coupling mechanisms responsible for the longitudinal structure of the equatorial ionosphere, *J. Geophys. Res.*, *115*, A05308, doi:10.1029/2009JA014894.

Foster, J. C. (1993), Storm time plasma transport at middle and high latitudes, *J. Geophys. Res.*, *98*(A2), 1675–1689, doi:10.1029/92JA02032.

Heise, S., N. Jakowski, A. Wehrenpfennig, C. Reigber, and H. Lühr (2002), Sounding of the topside ionosphere/plasmasphere based on GPS measurements from CHAMP: Initial results, *Geophys. Res. Lett.*, *29*(14), 1699, doi:10.1029/2002GL014738.

Immel, T. J., G. Crowley, C. L. Hackert, J. D. Craven, and R. G. Roble (2006), Effect of IMF B_y on thermospheric composition at high and middle latitudes: 2. Data comparisons, *J. Geophys. Res.*, *111*, A10312, doi:10.1029/2005JA011372.

Jakowski, N., S. Schluter, and E. Sardon (1999), Total electron content of the ionosphere during the geomagnetic storm on 10 January 1997, *J. Atmos. Sol. Terr. Phys.*, *61*, 299–307, doi:10.1016/S1364-6826(98)00130-8.

Kintner, P. M., T. Humphreys, and J. Hinks (2009), GNSS and ionospheric scintillation: How to survive the next solar maximum, *Inside GNSS*, *4*(4), 22–30.

Klobuchar, J. A. (1996), Ionospheric effects on GPS, in *Global Positioning System: Theory and Application*, vol. 1, *Prog. Astronaut. Aeronaut.*, vol. 163, edited by B. W. Parkinson and J. J. Spilker Jr., p. 485–516, Am. Inst. of Aeronaut. and Astronaut., Reston, Va.

Lin, C. H., J. Y. Liu, T. W. Fang, P. Y. Chang, H. F. Tsai, C. H. Chen, and C. C. Hsiao (2007), Motions of the equatorial ionization anomaly crests imaged by FORMOSAT-3/COSMIC, *Geophys. Res. Lett.*, *34*, L19101, doi:10.1029/2007GL030741.

Mannucci, A. J., B. D. Wilson, D. N. Yuan, C. H. Ho, U. J. Lindqwister, and T. F. Runge (1998), A global mapping technique for GPS-derived ionospheric total electron content measurements, *Radio Sci.*, *33*(3), 565–582, doi:10.1029/97RS02707.

Mitchell, C. N., L. Kersley, J. A. T. Heaton, and S. E. Pryse (1997), Determination of the vertical electron-density profile in ionospheric tomography: Experimental results, *Ann. Geophys.*, *15*, 747–752, doi:10.1007/s00585-997-0747-1.

Na, H. R., B. Hall, and E. Sutton (1995), Ground station spacing effects in ionospheric tomography, *Ann. Geophys.*, *13*, 1288–1296.

Pokhotelov, D., C. N. Mitchell, P. S. J. Spencer, M. R. Hairston, and R. A. Heelis (2008), Ionospheric storm time dynamics as seen by GPS tomography and in situ spacecraft observations, *J. Geophys. Res.*, *113*, A00A16, doi:10.1029/2008JA013109[Printed *114*(A3), 2009].

Pryse, S. E., C. N. Mitchell, J. A. T. Heaton, and L. Kersley (1995), Travelling ionospheric disturbance imaged by tomographic techniques, *Ann. Geophys.*, *13*, 1325–1342.

Raymund, T. D. (1995), Comparisons of several ionospheric tomography algorithms, *Ann. Geophys.*, *13*, 1254–1262.

Reinisch, B. W., D. M. Haines, R. F. Benson, J. L. Green, G. S. Sales, and W. W. L. Taylor (2001), Radio sounding in space: Magnetosphere and topside ionosphere, *J. Atmos. Sol. Terr. Phys.*, *63*(2–3), 87–98, doi:10.1016/S1364-6826(00)00133-4.

Stankov, S. M., N. Jakowski, S. Heise, P. Muhtarov, I. Kutiev, and R. Warnant (2003), A new method for reconstruction of the vertical electron density distribution in the upper ionosphere and plasmasphere, *J. Geophys. Res.*, *108*(A5), 1164, doi:10.1029/2002JA009570.

Tsai, L. C., C. H. Liu, W. H. Tsai, and C. T. Liu (2002), Tomographic imaging of the ionosphere using the GPS/MET and NNSS data, *J. Atmos. Sol. Terr. Phys.*, *64*, 2003–2011, doi:10.1016/S1364-6826(02)00218-3.

Valladares, C. E., and J. L. Chau (2012), The Low-Latitude Ionosphere Sensor Network: Initial results, *Radio Sci.*, *47*, RS0L17, doi:10.1029/2011RS004978.

Yizengaw, E., and M. B. Moldwin (2005), The altitude extension of the mid-latitude trough and its correlation with plasmapause position, *Geophys. Res. Lett.*, *32*, L09105, doi:10.1029/2005GL022854.

Yizengaw, E., E. A. Essex, and R. Birsa (2004), The Southern Hemisphere and equatorial region ionization response for 22 September 1999 severe magnetic storm, *Ann. Geophys.*, *22*(8), 2765–2773, doi:10.5194/angeo-22-2765-2004.

Yizengaw, E., M. B. Moldwin, P. L. Dyson, and T. J. Immel (2005), Southern Hemisphere ionosphere and plasmasphere response to the interplanetary shock event of 29–31 October 2003, *J. Geophys. Res.*, *110*, A09S30, doi:10.1029/2004JA010920.

Yizengaw, E., M. B. Moldwin, P. L. Dyson, and E. A. Essex (2007), Using tomography of GPS TEC to routinely determine ionospheric average electron density profiles, *J. Atmos. Sol. Terr. Phys.*, *69*, 314–321, doi:10.1016/j.jastp.2006.07.023.

Yizengaw, E., M. B. Moldwin, A. Mebrahtu, B. Damtie, E. Zesta, C. E. Valladares, and P. H. Doherty (2011), Comparison of storm time equatorial ionospheric electrodynamics in the African and American sectors, *J. Atmos. Sol. Terr. Phys.*, *73*(1), 156–163, doi:10.1016/j.jastp.2010.08.008.